Macromolecules

Article

pubs.acs.org/Macromolecules

Chain Propagation and Termination Mechanisms for Polymerization of Conjugated Polar Alkenes by [Al]-Based Frustrated Lewis Pairs

Jianghua He,[†] Yuetao Zhang,[†,‡] Laura Falivene,[§,∥] Lucia Caporaso,[∥] Luigi Cavallo,*[,§,∥] and Eugene Y.-X. Chen*[,†]

[†]Department of Chemistry, Colorado State University, Fort Collins, Colorado 80523-1872, United States

[‡]State Key Laboratory of Supramolecular Structure and Materials, College of Chemistry, Jilin University, Changchun 130012, China

[§]Physical Sciences and Engineering Division, Kaust Catalysis Center, King Abdullah University of Science and Technology (KAUST), Thuwal 23955-6900, Saudi Arabia

[∥]Dipartimento di Chimica e Biologia, Università di Salerno, Via Papa Paolo Giovanni II, I-84084 Fisciano, Italy

Supporting Information

ABSTRACT: A combined experimental and theoretical study on mechanistic aspects of polymerization of conjugated polar alkenes by frustrated Lewis pairs (FLPs) based on *N*-heterocyclic carbene (NHC) and $Al(C_6F_5)_3$ pairs is reported. This study consists of three key parts: structural characterization of active propagating intermediates, propagation kinetics, and chain-termination pathways. Zwitterionic intermediates that simulate the active propagating species in such polymerization have been generated or isolated from the FLP activation of monomers such as 2-vinylpyridine and 2-isopropenyl-2-oxazoline—one of which, $IMes^+$-$CH_2C(Me)=(C_3H_2NO)Al(C_6F_5)_3^-$ (**2**), has been structurally characterized. Kinetics performed on the polymerization of 2-vinylpyridine by $I^tBu/Al(C_6F_5)_3$ revealed that the polymerization follows a zero-order dependence on monomer concentration and a first-order dependence on initiator (I^tBu) and activator $[Al(C_6F_5)_3]$ concentrations, indicating a bimolecular, activated monomer propagation mechanism. The Lewis pair polymerization of conjugate polar alkenes such as methacrylates is accompanied by competing chain-termination side reactions; between the two possible chain-termination pathways, the one that proceeds via intramolecular backbiting cyclization involving nucleophilic attack of the activated ester group of the growing polymer chain by the *O*-ester enolate active chain end to generate a six-membered lactone (δ-valerolactone)-terminated polymer chain is kinetically favored, but thermodynamically disfavored, over the pathway leading to the β-ketoester-terminated chain, as revealed by computational studies.

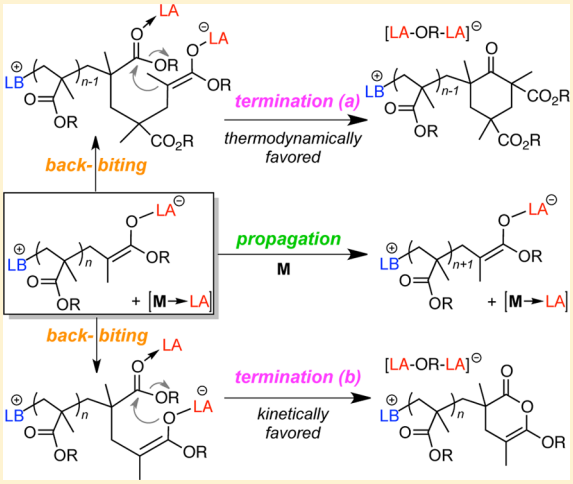

INTRODUCTION

The chemistry of "frustrated Lewis pairs" (FLPs) has attracted an explosive level of recent interest since the FLP concept was uncovered through the seminal works of Stephan and Erker.[1] A FLP was initially described as a nonclassical Lewis pair comprising a bulky Lewis acid (LA), such as $E(C_6F_5)_3$ (E = B, Al), and a bulky Lewis base (LB), such as P^tBu_3 and $PMes_3$ (Mes = 2,4,6-$Me_3C_6H_2$), that are sterically precluded from forming stable classical LB → LA adducts (CLAs). Nowadays, FLPs also include those Lewis pairs with a weak LB---LA bonds due to electronic frustration. Such FLPs exhibit the largely unquenched, orthogonal LA and LB reactivity that can promote unusual reactions, or reactions that were previously known to be possible only by transition-metal complexes, and display FLP-induced or enhanced reactivity in activation of small molecules, catalyzing the rapidly growing interest in the FLP chemistry.[1] In its relatively short history, the FLP chemistry has achieved remarkable successes in many areas of chemistry, chiefly activation of small molecules,[2] catalytic hydrogenation,[3] and new reactivity/reaction development.[4]

Lewis pair (LP) polymerization,[5] which utilizes either a CLA or a FLP in which the LA and LB work cooperatively to activate the monomer substrate and participate in chain initiation as well as chain propagation of termination/transfer events, has attracted recent interest in polymerization catalysis for the synthesis of several different classes of polymers. FLPs consisting of the bulky aluminum LA $Al(C_6F_5)_3$ and bulky phosphine or *N*-heterocyclic carbene (NHC) LBs have been utilized to initiate rapid polymerization of conjugated polar alkenes,[6] including linear and cyclic acrylic monomers such as

Received: September 18, 2014
Revised: October 21, 2014

   dx.doi.org/10.1021/ma5019389 | *Macromolecules* XXXX, XXX, XXX–XXX

Scheme 1. Proposed Chain Initiation and Propagation Mechanism for Polymerization of Conjugated Polar Alkenes Carrying a Functional Group (FG) by LPs[5,6,9] and a List of the Monomers Examined in This Study

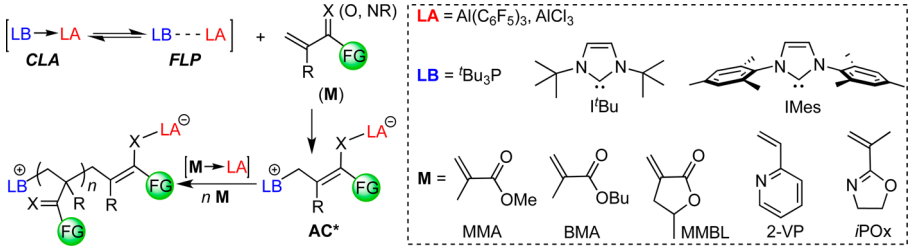

methyl methacrylate (MMA) as well as biorenewable α-methylene-γ-butyrolactone (MBL) and γ-methyl-α-methylene-γ-butyrolactone (MMBL), into high molecular weight (MW) polymers.[7] This polymerization was proposed to proceed through a bimolecular, activated monomer propagation mechanism via zwitterionic phosphonium or imidazolium enolaluminate active species (AC*, Scheme 1), which have been structurally characterized.[5,6] CLP adducts of phosphines (P) and boranes (B) have been found to exhibit unexpectedly high activity for the polymerization of MMBL, while the P/B FLPs exhibit negligible activity under the same conditions.[8] Conjugate-addition polymerization of the monomers bearing the C═C−C═N functionality, such as 2-vinylpyridine (2-VP) and 2-isopropenyl-2-oxazoline (*i*POx) (Scheme 1), is brought about effectively by NHC/Al(C_6F_5)$_3$ FLPs, but not by the related P/Al(C_6F_5)$_3$ FLPs.[9] The ring-opening (co)-polymerization of heterocyclic monomers such as lactide and lactones proceeds in a controlled manner in the presence of Zn(C_6F_5)$_2$-based LPs,[10] and the radical polymerization of styrene is mediated by the persistent FLP-NO aminoxyl radical derived from *N*,*N*-cycloaddition of a cyclohexylene-bridged intramolecular P---B FLP to nitric oxide.[11] LP cooperativity has been exploited to provide a facile approach for controlling regioselectivity of the polymerization of dissymmetric divinyl polar monomers such as 4-vinylbenzyl methacrylate producing soluble functional polymers.[12] Most recently, LPs based on *N*-heterocyclic olefins (NHO) as the LB and Al(C_6F_5)$_3$ or $AlCl_3$ as the LA have also been found to be highly active for the polymerization of conjugated polar alkenes such as methacrylates and acrylamides; deactivation of the active propagating species (the imidazolium enolaluminate) was proposed to lead to the polymer chains end-capped by the six-membered lactone, presumably resulted from nucleophilic backbiting of the polymeric enolaluminate anion to the carboxyl carbon of the adjacent unit, with concomitant release of the methoxyl group.[13]

The studies overviewed above have resulted in significant recent progress in polymerization catalysis by FLPs or CLAs. However, although the chain initiation and propagation events as well as the scope of monomer and LPs have been examined in great detail,[6,9] polymerization kinetics and chain-termination mechanisms for the polymerization of conjugated polar alkenes, such as MMA, MMBL, 2-VP, and *i*POx, by FLPs based on NHC bases and [Al] acids have not been reported. Such fundamental insight will undoubtedly enhance our understanding of the polymerization by FLPs in terms of the mechanism of chain growth vs termination and polymer chain end structures, which will guide the design of more effective LPs for such polymerization reactions. Hence, the central objective of this work was to investigate the kinetics and chain-termination mechanism of the polymerization of typical conjugated polar alkenes by FLPs, using two prototype systems: I^{t}Bu/Al(C_6F_5)$_3$ and IMes/Al(C_6F_5)$_3$.

EXPERIMENTAL SECTION

Materials, Reagents, and Methods. All syntheses and manipulations of air- and moisture-sensitive materials were carried out in flamed Schlenk-type glassware on a dual-manifold Schlenk line, on a high-vacuum line, or in an inert gas-filled glovebox. NMR-scale reactions were conducted in Teflon-valve-sealed J. Young-type NMR tubes. HPLC-grade organic solvents were first sparged extensively with nitrogen during filling 20 L solvent reservoirs and then dried by passage through activated alumina (for Et_2O, THF, and CH_2Cl_2) followed by passage through Q-5 supported copper catalyst (for toluene and hexanes) stainless steel columns. Benzene-d_6 and toluene-d_8 were dried over sodium/potassium alloy and vacuum-distilled or filtered, whereas CD_2Cl_2 and $CDCl_3$ were dried over activated Davison 4 Å molecular sieves. HPLC-grade dimethylformamide (DMF) was degassed and dried over CaH_2 overnight, followed by vacuum distillation (CaH_2 was removed before distillation). NMR spectra were recorded on Varian Inova 300 (300 MHz, ^{1}H; 75 MHz, ^{13}C; 282 MHz, ^{19}F) or a Varian 400 MHz spectrometer. Chemical shifts for ^{1}H and ^{13}C spectra were referenced to internal solvent resonances and are reported as parts per million relative to $SiMe_4$, whereas ^{19}F NMR spectra were referenced to external $CFCl_3$.

Methyl methacrylate (MMA), 2-isopropenyl-2-oxazoline (*i*POx), 2-vinylpyridine (2-VP), and *n*-butyl methacrylate (BMA) were purchased from Sigma-Aldrich Co., while γ-methyl-α-methylene-γ-butyrolactone (MMBL) was purchased from TCI America. These monomers were first degassed and dried over CaH_2 overnight, followed by vacuum distillation. Further purification of MMA involved titration with neat tri(*n*-octyl)aluminum to a yellow end point,[14] followed by distillation under reduced pressure. All purified monomers were stored in brown bottles and stored inside a glovebox freezer at −30 °C. *N*-Heterocyclic carbenes (NHCs), including 1,3-bis(2,4,6-trimethylphenyl)imidazol-2-ylidene (IMes) and 1,3-di-*tert*-butylimidazol-2-ylidene (I^{t}Bu), were purchased from Strem Chemical Co. Phosphines, including $PMes_3$, PPh_3, and P^{t}Bu$_3$, as well as butylated hydroxytoluene (BHT-H, 2,6-di-*tert*-butyl-4-methylphenol) were purchased from Alfa Aesar Chemical Co. BHT-H was recrystallized from hexanes prior to use. P^{t}Bu$_3$ was first degassed and dried over CaH_2 overnight, followed by vacuum distillation. Tris(pentafluorophenyl)borane, B(C_6F_5)$_3$, obtained as a research gift from Boulder Scientific Company, was further purified by recrystallization from hexanes at −30 °C. Al(C_6F_5)$_3$, as a (toluene)$_{0.5}$ adduct, denoted as [Al], was prepared by reaction of B(C_6F_5)$_3$ and $AlMe_3$ in a 1:3 toluene/hexanes solvent mixture in quantitative yield;[15] this is the modified synthesis based on literature procedures.[16] Although we have experienced no incidents when handling this material, *extra caution should be exercised*, especially when dealing with the unsolvated form because of its thermal and shock sensitivity.

Isolation of Adduct *i*POx·Al(C_6F_5)$_3$ (1). Adduct **1** was isolated as an off-white solid in quantitative yield using the same procedure as described for the isolation of the adduct (2-VP)·Al(C_6F_5)$_3$.[9] ^{1}H NMR (C_6D_6, 23 °C): δ 5.43 (br s, 1H, C*H*$_2$=), 4.62 (br s, 1H, C*H*$_2$=), 3.25 (t, *J* = 9.3 Hz, 2H, C*H*$_2$−O), 3.07 (t, *J* = 9.3 Hz, 2H, C*H*$_2$−N), 1.28 (s,

dx.doi.org/10.1021/ma5019389 | *Macromolecules* XXXX, XXX, XXX−XXX

3H, CH_3−). ^{19}F NMR (C_6D_6, 23 °C): δ −122.6 (d, J = 16.6 Hz, 6F, o-F), −152.2 (t, J = 19.7 Hz, 3F, p-F), −161.1 (m, 6F, m-F).

***In Situ* Generation of Imidazolium Oxazolinylaluminate IMes$^+$-CH_2C(Me)═(C_3H_2NO)Al(C_6F_5)$_3^-$ (2).** A Teflon-valve-sealed J. Young-type NMR tube was charged with IMes (17.4 mg, 57.0 mmol) and 0.3 mL of C_7D_8. A 0.3 mL C_7D_8 solution of *i*POx·Al(C_6F_5)$_3$ (36.4 mg, 57.0 mmol) was added to this tube via pipet at ambient temperature. The resulting colorless mixture was allowed to react for 10 min before analysis by NMR, which showed the clean and quantitative formation of zwitterionic species **2**. ^{1}H NMR (C_7D_8, 23 °C): δ 6.60 (s, 4H, Ph), 5.71 (s, 2H, NC*H*=), 3.38 (br s, 4H, CH_2), 2.98 (s, 2H, CH_2), 1.61 (s, 12H, Ph−*Me*), 1.20 (s, 3H, =C*Me*). ^{19}F NMR (C_7D_8, 23 °C): δ −121.9 (d, J = 18.0 Hz, 6F, o-F), −157.3 (t, J = 19.6 Hz, 3F, p-F), −163.5 (m, 6F, m-F). ^{13}C NMR (C_7D_8, 23 °C): δ 159.4, 151.8, 140.8, 133.8, 130.2, 129.4, 121.4, 65.0, 62.6, 49.7, 29.4, 20.3, 18.5, 16.6.

X-ray Crystallographic Analysis of IMes$^+$-CH_2C(Me)═(C_3H_2NO)Al(C_6F_5)$_3^-$ (2). The molecular structure of **2** has been confirmed by single crystal X-ray diffraction analysis. A 20 mL glass vial was charged with *i*POx·Al(C_6F_5)$_3$ (0.16 mmol) and 4 mL of CH_2Cl_2, while another vial was charged with IMes (0.16 mmol) and 10 mL of hexanes. The two vials were cooled to −30 °C, and the solution of IMes was layered on the *i*POx·Al(C_6F_5)$_3$ solution via pipet at low temperature. The vial was stored in the glovebox freezer at −30 °C for 1 week to afford single crystals of **2** suitable for X-ray diffraction analysis. The crystals were quickly covered with a layer of Paratone-N oil (Exxon, dried and degassed at 120 °C/10^{-6} Torr for 24 h) after decanting the mother liquor. A crystal was then mounted on a thin glass fiber and transferred into the cold nitrogen stream of a Bruker SMART CCD diffractometer. The structure was solved by direct methods and refined using the Bruker SHELXTL program library.[17] The structure was refined by full-matrix least-squares on F^2 for all reflections. All non-hydrogen atoms were refined with anisotropic displacement parameters, whereas hydrogen atoms were included in the structure factor calculations at idealized positions. Selected crystallographic data for **2**: $C_{45}H_{33}AlF_{15}N_3O$, monoclinic, space group $P2(1)/c$, a = 11.7821(14) Å, b = 18.266(2) Å, c = 19.231(2) Å, β = 96.320(6)°, V = 4113.7(8) Å^3, Z = 4, D_{calcd} = 1.524 mg/m^3, GOF = 1.047, $R1$ = 0.0426 [$I > 2(I)$], $wR2$ = 0.11185 (all data). CCDC-972836 contains the supplementary crystallographic data for this structure. These data can be obtained free of charge from The Cambridge Crystallographic Data Centre via www.ccdc.cam.ac.uk/data_request/cif.

***In Situ* Generation of Imidazolium Oxazolinylaluminate I^{t}Bu$^+$-CH_2C(Me)═(C_3H_2NO)Al(C_6F_5)$_3^-$ (3).** A Teflon-valve-sealed J. Young-type NMR tube was charged with I^{t}Bu (8.5 mg, 47 mmol) and 0.3 mL of C_6D_6. A 0.3 mL C_6D_6 solution of *i*POx·Al(C_6F_5)$_3$ (30 mg, 47 mmol) was added to this tube via pipet at ambient temperature. The resulting colorless mixture was allowed to react for 10 min before analysis by NMR, which showed the clean and quantitative formation of zwitterionic species **3** as two isomers A (major) and B (minor) in a 2:1 ratio. ^{1}H NMR (C_6D_6, 23 °C) for **3**A: δ 6.18 (s, 2H, NC*H*=), 4.05−3.26 (m, 6H, CH_2), 1.64 (s, 3H, Me), 1.00 (s, 18H, ^{t}Bu); **3**B: δ 6.02 (s, 2H, NC*H*=), 4.05−3.26 (m, 6H, CH_2), 1.24 (s, 3H, Me), 0.91 (s, 18H, ^{t}Bu). ^{19}F NMR (C_6D_6, 23 °C) for **3**A: δ −122.0 (d, J = 16.9 Hz, 6F, o-F), −157.1 (t, J = 19.7 Hz, 3F, p-F), −163.4 (m, 6F, m-F); **3**B: δ −121.4 (d, J = 18.6 Hz, 6F, o-F), −156.6 (t, J = 19.7 Hz, 3F, p-F), −162.9 (m, 6F, m-F). ^{13}C NMR (C_6D_6, 23 °C) for **3**A: δ 157.6, 148.0, 116.8, 67.7, 65.6, 61.8, 49.1, 31.0, 28.8, 14.2; **3**B: δ 159.7, 148.3, 117.0, 66.7, 65.6, 62.3, 55.0, 31.0, 28.6, 19.2.

Isolation of Imidazolium Pyridylaluminate I^{t}Bu$^+$-CH_2CH═(C_5H_4N)Al(C_6F_5)$_3^-$ (4). A 20 mL glass vial was charged with I^{t}Bu (0.17 g, 0.95 mmol) and 5 mL of toluene, while another vial was charged with (2-VP)·Al(C_6F_5)$_3$ (0.50 g, 0.79 mmol) and 10 mL of toluene. The two vials were mixed via pipet at ambient temperature to give a red suspension. The solvent was removed, and the solid residue was washed by hexanes (3 × 5 mL) to give **4** as an orange-red solid in quantitative yield after drying under vacuum. The spectral and X-ray structural data were reported previously.[9]

General Polymerization Procedures. Polymerizations were performed either in 25 mL flame-dried Schlenk flasks interfaced to the dual-manifold Schlenk line for runs using external temperature bath or in 30 mL glass reactors inside the glovebox for ambient temperature (ca. 25 °C) runs. In a typical polymerization procedure, a predetermined amount of a LA or its monomer adduct, such as [Al], *i*POx·Al(C_6F_5)$_3$, (2-VP)·Al(C_6F_5)$_3$, or B(C_6F_5)$_3$, was first dissolved in a monomer (0.5 mL for *i*POx or 0.51 mL for 2-VP, 200 equiv relative to the LB) and 3.1 mL of solvent (CH_2Cl_2 or toluene) inside a glovebox. Benzene (0.369 g, 4.73 mmol) was added as an internal standard to each reactor if needed. The polymerization was started by rapid addition of a solution of a LB (1 equiv of a phosphine or an NHC) in 1.0 mL of solvent (CH_2Cl_2 or toluene) via a gastight syringe to the above mixture containing the LA and monomer under vigorous stirring. The amount of the monomer was fixed for all polymerization. After the measured time interval, a 0.2 mL aliquot was taken from the reaction mixture via syringe and quickly quenched into a 4 mL vial containing 0.6 mL of undried "wet" $CDCl_3$ stabilized by 250 ppm of BHT-H; the quenched aliquots were later analyzed by ^{1}H NMR to obtain the percent monomer conversion data. After the polymerization was stirred for the stated reaction time, then the polymer was immediately precipitated into 200 mL of hexane, stirred for 1 h, filtered, washed with hexane, and dried in a vacuum oven at 50 °C overnight to a constant weight.

Polymerization Kinetics. Kinetic experiments were carried out in a stirred glass reactor at ambient temperature (ca. 25 °C) inside an argon-filled glovebox using the polymerization procedure already described above, with [Al]/[I^{t}Bu] ratios of 1.5:0.5, 2:1, 2.5:1.5, and 3:2, [2-VP]$_0$ was fixed at 946 mM for all polymerizations, where I^{t}Bu = 2.38, 4.77, 7.16, and 9.54 mM and [Al] = 7.17, 9.54, 11.9, and 14.3 mM in 5 mL mixture solutions. Benzene was added an internal standard to each reactor. At appropriate time intervals, 0.2 mL aliquots were withdrawn from the reaction mixture using a syringe and quickly quenched into 4 mL septum-sealed vials containing 0.6 mL of undried "wet" $CDCl_3$ mixed with 250 ppm BHT-H. The quenched aliquots were analyzed by ^{1}H NMR for determining the ratio of [2-VP]$_t$ at a given time t to [2-VP]$_0$, [2-VP]$_t$:[2-VP]$_0$. Apparent rate constants (k_{app}) were extracted from the slopes of the best fit lines to the plots of [2-VP]$_t$:[2-VP]$_0$ vs time. Another set of kinetic experiments were carried out to determine the kinetic order with respect to [Al]. In these experiments, the ratio of [2-VP]$_0$:[**4**]$_0$ was fixed at 200:1, with [2-VP]$_0$ = 946 mM and [**4**]$_0$ = 4.73 mM for all polymerizations. The [Al]$_0$:[**4**]$_0$ ratio was varied as 0.2:1, 0.4:1, 0.6:1, 0.8, and 1:1, where [**4**]$_0$ = 4.73 mM and [Al]$_0$ = 0.944, 1.89, 2.83, 3.78, and 4.73 mM in 5 mL of total solutions. Benzene was added an internal standard to each reactor. The rest of the procedure was the same as described above.

Polymer Characterizations. Polymer number-average molecular weights (M_n) and molecular weight distributions ($Đ = M_w/M_n$) were measured by gel permeation chromatography (GPC) analyses carried out at 40 °C and a flow rate of 1.0 mL/min, with DMF as the eluent, on a Waters University 1500 GPC instrument equipped with one PLgel 5 μm guard and three PLgel 5 μm mixed-C columns (Polymer Laboratories; linear range of molecular weight = 200−2 000 000). The instrument was calibrated with 10 PMMA standards, and chromatograms were processed with Waters Empower software (version 2002).

The isolated low-MW polymer samples were analyzed by matrix-assisted laser desorption/ionization time-of-flight mass spectroscopy (MALDI-TOF MS); the experiment was performed on a Ultralex MALDI-TOF mass spectrometer (Bruker Daltonics) operated in positive ion, reflector mode using a Nd:YAG laser at 355 nm and 25 kV accelerating voltage. A thin layer of a 1% NaI solution was first deposited on the target plate, followed by 0.6 μL of both sample and matrix (dithranol, 10 mg/mL in 50% CAN, 0.1% TFA). External calibration was done using a peptide calibration mixture (4−6 peptides) on a spot adjacent to the sample. The raw data were processed in the FlexAnalysis software (version 2.4, Bruker Daltonics).

Computational Methods. All the density functional theory (DFT) calculations were performed using the Gaussian09 package and followed the procedures described in our prior publications.[18] Geometry optimizations were performed with the BP86 GGA

dx.doi.org/10.1021/ma5019389 | Macromolecules XXXX, XXX, XXX−XXX

functional of Becke and Perdew,[19,20] and the standard split-valence basis set with a polarization function of Ahlrichs and co-workers (SVP keyword in Gaussian) was used.[21] The reported energies have been obtained via single point energy calculations on the optimized geometries with the M06 functional with the triple-ζ basis set of Ahlrichs (TZVP keyword in Gaussian09). The solvent (toluene) effects were included with the default Gaussian PCM implementation.[22] Thermal corrections from gas-phase frequency analysis, performed with the BP86 functional and the SVP basis set on the BP86 optimized geometries, were added to this in solvent energy to obtain the free energies.

RESULTS AND DISCUSSION

Generation and Structural Characterization of Zwitterionic Intermediate 2. NHC/Al(C_6F_5)$_3$ FLPs have been found to be active for polymerization of *i*POx, producing medium high molecular weight polymers with M_n = 7.37 × 10^4 g/mol (NHC = I^{t}Bu) and M_n = 1.50 × 10^4 g/mol (NHC = IMes).[9] The polymers P*i*POx produced exhibited a broad molecular weight distribution of $Đ \sim 3.0$, showing that the polymerization of *i*POx by the Al-based FLPs is less controlled than the group-transfer polymerization catalyzed by rare-earth metal complexes.[23] Nonetheless, it is of fundamental interest to understand the active species responsible for this polymerization by FLPs.

Reaction of *i*POx·Al(C_6F_5)$_3$ (**1**) with IMes at RT in C_7D_8 cleanly generates the corresponding zwitterionic imidazolium oxazolinylaluminate IMes$^+$-$CH_2C(Me)$=(C_3H_2NO)Al-(C_6F_5)$_3^-$ (**2**, Scheme 2), as readily characterized by NMR

Scheme 2. Generation of Zwitterionic Intermediate 2 from Activation of *i*POx by IMes/Al(C_6F_5)$_3$

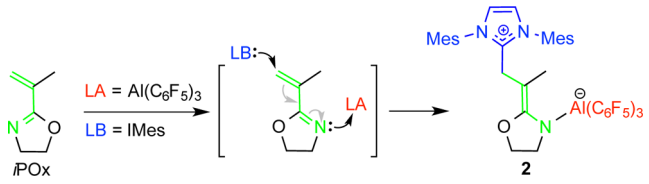

spectroscopy (see Experimental Section). Most notable spectral features manifesting this transformation include (a) conversion of the sp^2-olefinic =CH_2 in the monomer or its LA adduct **1** (δ 5.43, 4.62 ppm) to the sp^3-methylene (−CH_2−) group in **2** (δ 2.98 ppm) as shown by ^{1}H NMR; (b) disappearance of the characteristic NMR signal for the carbene moiety at C(2) (δ 219.7 ppm) in the NHC IMes upon its reaction with the [Al] activated monomer as shown by ^{13}C NMR; and (c) high-field shifted *para*- and *meta*-fluorine resonances by 5.1 and 2.4 ppm (to δ −157.3 and −163.5 ppm, respectively) in the ^{19}F NMR spectrum (relative to [Al] or its monomer adduct **1**), characteristic of the aluminate formation. Replacing IMes with I^{t}Bu for the same reaction led to formation of the analogous zwitterionic imidazolium oxazolinylaluminate I^{t}Bu$^+$-$CH_2C(Me)$=$(C_3H_2NO)Al(C_6F_5)_3^-$ (**3**); however, this reaction gave two double-bond (*E* and *Z*) isomers in a 2:1 ratio (see Experimental Section).

The molecular structure of **2** (Figure 1) has been confirmed by single-crystal X-ray diffraction analysis. It is clear from the diffraction data that, as a consequence of conjugate addition of IMes to adduct **1**, a double bond is formed between C(5) and C(7) in **2** with a bond length of 1.343 (3) Å, whereas a single bond is formed between C(4) and C(5) [1.509(3) Å], from a previous C=C double bond, as well as between C(1) and C(4)

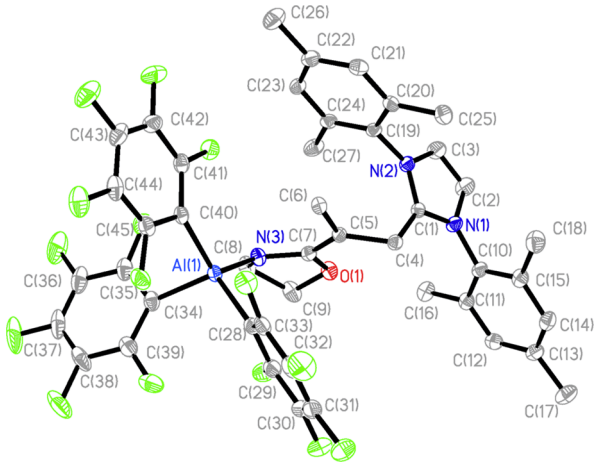

Figure 1. X-ray crystal structure of zwitterionic intermediate **2**. Hydrogen atoms have been omitted for clarity and ellipsoids drawn at 50% probability. Selected bond lengths [Å] and angles [deg]: Al(1)−N(3) 1.8534(17), Al(1)−C(40) 2.022(2), Al(1)−C(28) 2.023(2), Al(1)−C(34) 2.023(2), C(1)−C(4) 1.499(3), C(4)−C(5) 1.509(3), C(5)−C(7) 1.343(3); N(3)−Al(1)−C(40) 118.36(8), N(3)−Al(1)−C(28) 106.94(8), C(40)−Al(1)−C(28) 112.22(8), N(3)−Al(1)−C(34) 108.04(8), C(40)−Al(1)−C(34) 97.92(8), C(28)−Al(1)−C(34) 113.26(9).

[1.499(3) Å], for the newly formed σ-bond between IMes and *i*POx. This structure represents one of only a handful of structurally characterized zwitterionic intermediates that simulate the active propagating species for the Lewis pair polymerization, including those zwitterionic intermediates derived from FLP activation of monomers such as MMA,[6] MBL,[6] and 2-VP.[9]

Kinetics of Polymerization by I^{t}Bu/Al(C_6F_5)$_3$. To investigate the kinetics of the polymerization of conjugated polar alkenes by FLPs, we initially examined several monomers and FLPs for their suitability for kinetic studies and finally arrived at the polymerization of 2-VP by I^{t}Bu/Al(C_6F_5)$_3$ because its polymerization rate and ability to cleanly generate the isolable, active zwitterionic intermediate (i.e., **4**) were found most suitable for the kinetic study using the method employed in this study. Accordingly, we examined kinetics of the 2-VP polymerization by I^{t}Bu/Al(C_6F_5)$_3$ in toluene at RT with two different sets of experiments. In the first set of kinetic experiments, the alane [Al] was dissolved in a fixed amount of 2-VP (946 mM for all polymerizations) and toluene, and the polymerization was started by addition of I^{t}Bu. The [Al]/[I^{t}Bu] ratio was varied at 1.5:0.5, 2:1, 2.5:1.5, and 3:2 such that at each ratio there was 1 equiv of the LA [Al] left to activate the monomer upon formation of 1 equiv of the zwitterionic species that consumes equimolar LB and LA. As can be seen from a representative kinetic plot for the 2-VP polymerization by [Al]/I^{t}Bu in a 2.5/1.5 ratio, the polymerization clearly followed zero-order kinetics with respect to [2-VP] concentration (Figure 2); the same zero-order dependence was observed for all the [Al]/I^{t}Bu ratios investigated in this study (Figure S1a−d). A double-logarithm plot (Figure 3) of the apparent rate constants (k_{app}), obtained from the slopes of the best-fit lines to the plots of $[2\text{-VP}]_t/[2\text{-VP}]_0$ vs time, as a function of ln[I^{t}Bu] was fit to a straight line (R^2 = 0.991) with slope = 1.08, revealing that the propagation is first order in the LB concentration, [I^{t}Bu].

In the second set of kinetic experiments, we employed the pregenerated, isolated zwitterionic imidazolium pyridylalumi-

dx.doi.org/10.1021/ma5019389 | Macromolecules XXXX, XXX, XXX−XXX

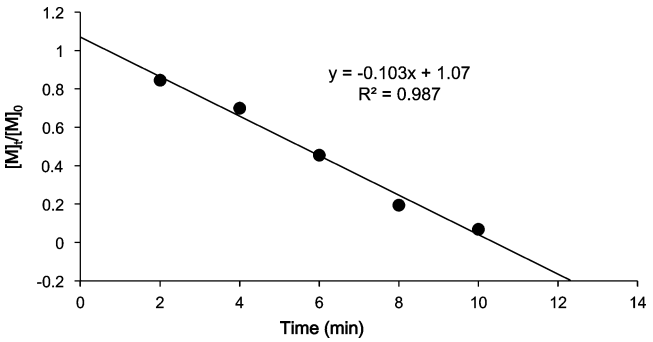

Figure 2. Zero-order plot of $[2\text{-VP}]_t/[2\text{-VP}]_0$ vs time for the polymerization of 2-VP by $Al(C_6F_5)_3/I^tBu$ (2.5/1.5) in toluene at RT. Conditions: $[2\text{-VP}]_0$ = 946 mM, $[Al]_0$ = 11.9 mM, $[I^tBu]_0$ = 7.16 mM in 5 mL solution. Similar plots with other $[Al]/[I^tBu]$ ratio runs were depicted in Figure S1a–d.

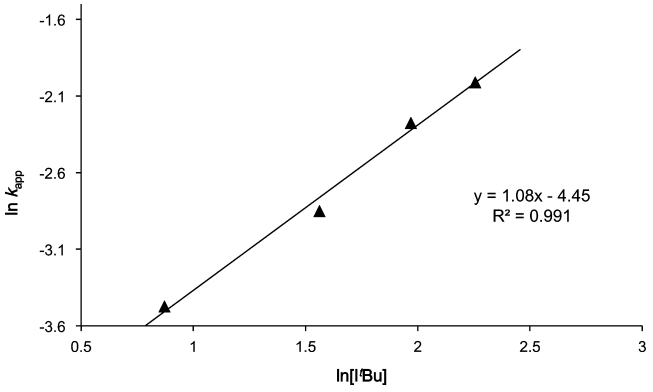

Figure 3. Plot of $\ln(k_{app})$ vs $\ln[I^tBu]$ for the 2-VP polymerization by $Al(C_6F_5)_3/I^tBu$ in toluene at RT.

nate $I^tBu\text{-}CH_2CH{=}(C_5H_4N)Al(C_6F_5)_3$ (**4**), in combination with a varied amount of [Al] to examine the kinetic order with respect to [Al]. Specifically, the [Al]/[**4**] ratio was varied from 0.2, 0.4, 0.6, 0.8, to 1.0, while keeping the [2-VP]:[**4**] ratio fixed at 200:1. While the rate of the polymerization was significantly enhanced with an increase in the [Al]/[**4**] ratio from 0.2 to 1.0, the molecular weight of the isolated resulting polymer PVP upon achieving quantitative monomer conversion did not follow this trend: M_n = 174 kg/mol, $Đ$ = 1.91 (ratio = 0.2); M_n = 95.4 kg/mol, $Đ$ = 1.45 (ratio = 0.4); M_n = 116 kg/mol, $Đ$ = 1.40 (ratio = 0.6 ratio); M_n = 90.4 kg/mol, $Đ$ = 1.44 (ratio = 0.8); M_n = 88.3 kg/mol, $Đ$ = 1.44 (ratio = 1.0). It is clear that the MW of the polymer obtained from all the ratio runs was much higher than the calculated (M_n = 21.0 kg/mol), thus giving rise to low initiator efficiencies from 12% to 24%; however, the highest MW polymer (thus the lowest initiator efficiency of 12%) achieved at the lowest [Al]/[**4**] ratio (0.2) and the lowest MW polymer (thus the highest initiator efficiency of 24%) obtained at the highest [Al]/[**4**] ratio (1.0) are consistent with the reasoning that a higher amount of the free [Al] in the solution promotes more efficient chain initiation and faster chain propagation, characteristic of an activated monomer polymerization process.[24] Kinetic plots for this set of kinetic experiments again showed that the propagation is zero order in [2-VP] for all the [Al]/[**4**] ratios investigated in this study (Figure S2a–e). A double-logarithm plot (Figure 4) of the apparent rate constants (k_{app}), obtained from the slopes of the best-fit lines to the plots of $[2\text{-VP}]_t/[2\text{-VP}]_0$ vs time, as a function of ln[Al] was fit to a straight line (R^2 = 0.980) with a slope of 0.977. Thus, the kinetic order with respect to [Al], given by the slope of ∼1, reveals that the propagation is also first-order in the LA concentration, [Al].

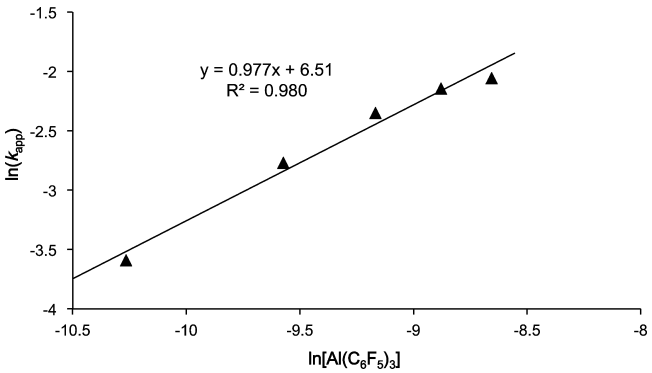

Figure 4. Plot of $\ln(k_{app})$ vs ln[Al] for polymerization of 2-VP by **4**/$Al(C_6F_5)_3$.

Overall, the 2-VP polymerization by the $I^tBu/Al(C_6F_5)_3$ pair follows a bimolecular, activated monomer propagation mechanism, as previously predicted by a computational study for the MMA polymerization by the $LB/Al(C_6F_5)_3$.[6a] Noteworthy is that such polymerization kinetics (i.e., zero-order dependence on monomer concentration and first-order dependence on initiator and LA activator concentrations) were also observed in the group-transfer polymerization catalyzed by zirconocenium cations[25] and silylium ions.[26] Such kinetics are consistent with the propagation mechanism in that the C–C bond forming step via intermolecular Michael addition of the propagating species to the LA-activated monomer is the rate-limiting step and the release of the LA catalyst from its coordinated last inserted monomer unit in the growing polymer chain to the incoming monomer is relatively fast.[24]

Chain Termination in the Polymerization by IMes/$Al(C_6F_5)_3$. The above 2-VP polymerization results reiterated the common theme observed from the polymerization of other conjugated polar alkenes such as MMA and MMBL by CLPs or FLPs:[6,9] such polymerization is hampered by chain-termination side reactions, chiefly evidenced by the much higher observed M_n than the calculated M_n (which results in low initiator efficiencies of typically lower than 30%), broad molecular weight distributions of the resulting polymers, and the inability to produce well-defined block copolymers via sequential copolymerization. The two possible chain-termination pathways that compete with chain propagation cycles are proposed in Scheme 3. Pathway (a) is proposed to proceed via intramolecular backbiting cyclization involving nucleophilic attack of the activated *antepenultimate* ester group of the growing polymer chain by the *C*-ester enolate active chain end to generate a cyclic *β*-ketoester-terminated polymer chain. This mode of backbiting cyclization was observed previously in the polymerization of acrylates by a metallocenium catalyst[27] and is also ubiquitous in the anionic polymerization of acrylates.[28] Pathway (b) is proposed to proceed via intramolecular backbiting cyclization involving nucleophilic attack of the activated *adjacent* ester group of the growing polymer chain by the *O*-ester enolate active chain end to generate a six-membered lactone (*δ*-valerolactone)-terminated polymer chain. This possible mode of chain termination was recently

dx.doi.org/10.1021/ma5019389 | Macromolecules XXXX, XXX, XXX–XXX

Scheme 3. Proposed Two Possible Backbiting Chain-Termination Pathways That Compete with Chain Propagation Cycles in the Polymerization of Methacrylates by the LB/LA Pair [LB = IMes, LA = $Al(C_6F_5)_3$ in the Following Examples]

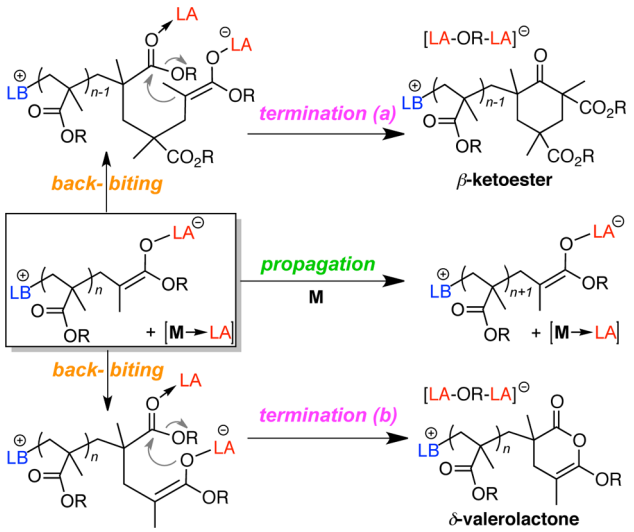

reported to be operative in the MMA polymerization by NHO/$Al(C_6F_5)_3$.[13]

To probe these chain-termination side reactions in the conjugate-addition polymerization by LB/LA pairs, we analyzed the chain-end groups of the low-MW polymers (PBMA and PMMBL) produced by such pairs. As can be seen from Figure 5, the MALDI-TOF MS spectrum of the low-MW PBMA sample consisted of two series of mass ions with rather similar intensities, with the spacing of the mass ions within each series being that of the value for PBMA repeat unit (m/z = 142). A plot of m/z values for series A in the MS spectrum vs the number of BMA repeat units (n) afforded a straight line with a slope of 142.09 and an intercept of 305.21 (Figure 6); the slope corresponds to the mass of the BMA monomer, whereas the intercept is the sum of the masses of IMes (304) and H (1) moieties, where IMes was derived from the chain initiation by IMes and H was derived from the acidic work-up after the polymerization. In short, the peaks in series A correspond to the linear, living polymer chain produced by IMes/$Al(C_6F_5)_3$.

A linear plot of m/z values for series B in the MS spectrum vs the BMA repeat units (n) gave the same slope but a different

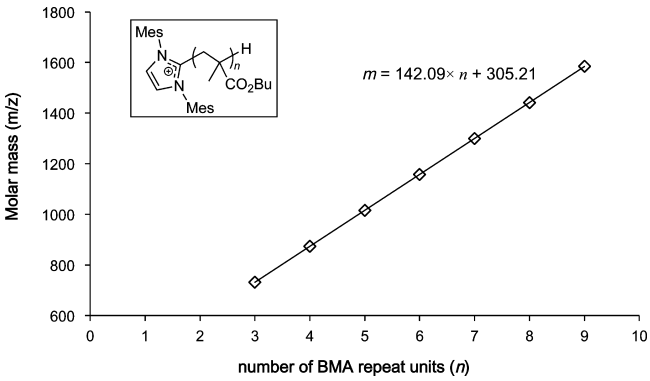

Figure 6. Plot of m/z values from Figure 5 vs the number of BMA repeat units (n) for A series.

intercept of 373.44 (Figure 7). A closer examination of these two series of mass ions revealed that the mass difference

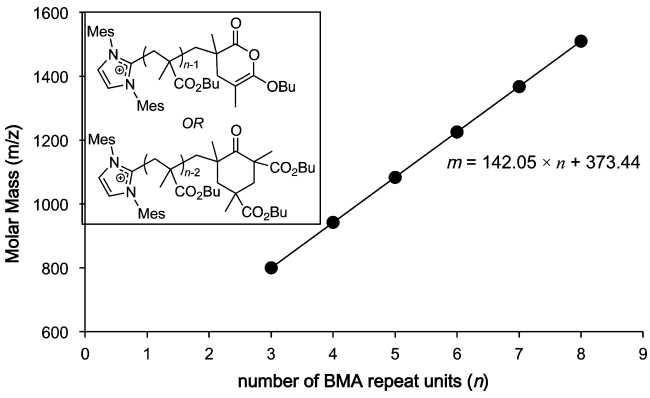

Figure 7. Plot of m/z values from Figure 5 vs the number of BMA repeat units (n) for B series.

between the linear polymer chain structure mass ions (series A) and the structure with the proposed cyclic chain end (series B) is a mass equivalent of ^{n}BuOH. Thus, the intercept of the B series plot is the sum of the masses of IMes and the cyclic β-ketoester moieties, where IMes was derived from the chain initiation by IMes (304) and the cyclic β-ketoester [142 (BMA) − 73 (loss of BuO) = 69] was derived from the backbiting chain-termination process during the polymerization (Scheme 3). Another low-MW PBMA sample produced by IMes/

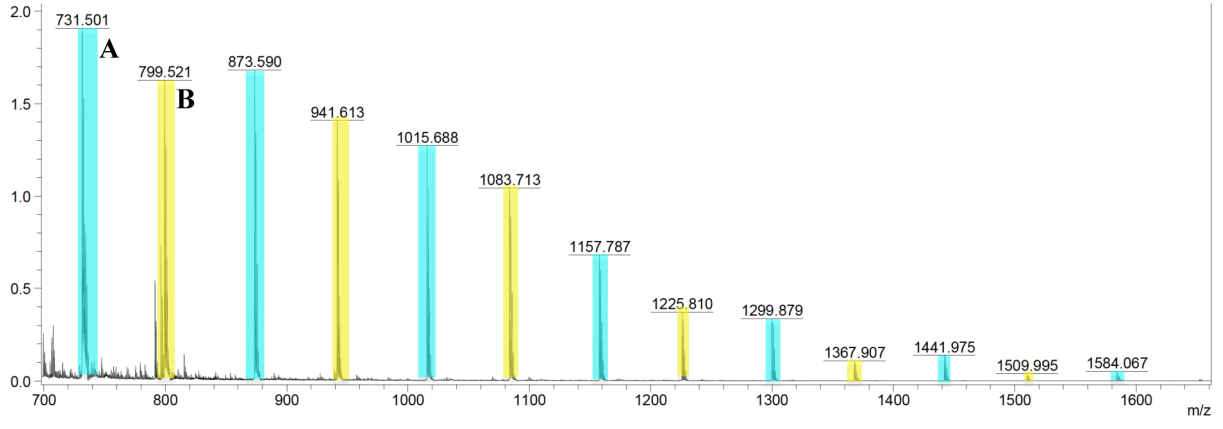

Figure 5. MALDI-TOF mass spectrum of the low-MW PBMA produced by IMes/$Al(C_6F_5)_3$ (1/2) in toluene at room temperature.

dx.doi.org/10.1021/ma5019389 | Macromolecules XXXX, XXX, XXX−XXX

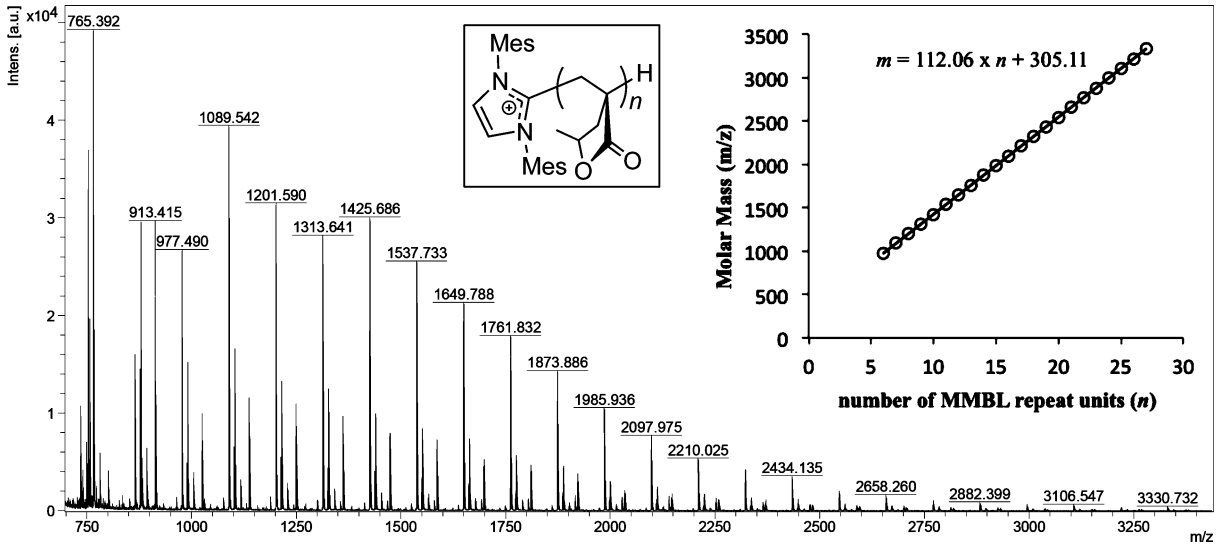

Figure 8. MALDI-TOF mass spectrum of the low-MW PMMBL produced by IMes/Al(C_6F_5)$_3$ (1/2) in toluene at RT. Inset: plot of m/z values of the main series vs the number of MMBL repeat units (n).

Al(C_6F_5)$_3$ at 0 °C gave a similar MALDI-TOF mass spectrum (Figure S3). It should be noted here that the MALDI-TOF MS results cannot differentiate between the possible cyclic β-ketoester and δ-valerolactone chain ends as the mass difference is one monomer unit (Scheme 3). However, DFT calculations detailed in the following indicated a clear kinetic preference for the formation of the cyclic δ-valerolactone chain end.

We reasoned that MMBL, being the cyclic analogue of the linear methacylates, should be more resistant toward chain termination via backbiting due to its robust, five-membered cyclic structure. Indeed, the MALDI-TOF MS spectrum of the low-MW PMMBL produced by IMes/Al(C_6F_5)$_3$ (1/2) showed one major series of mass ions. A plot of m/z values of this series vs the number of MMBL repeat units (n) yielded a straight line with a slope of 112.06 (mass of MMBL) and an intercept of 305.11 (Figure 8); again, the intercept is the sum of the masses of IMes and H moieties, indicating that the majority of the polymer chains produced in this polymerization is the linear, living chain. However, two minor series of mass ions were also present in the MS spectrum, indicative of side reactions such as chain termination or transfer; one of such series gave a structure without apparent chain ends (with an intercept being the mass of Na^+), which is consistent with a scenario that chain transfer to monomer occurs through deprotonation of the MMBL monomer by the propagating enolate anion, and the resulting anionic monomer initiates new chains, as shown in the related organocatalytic polymerization system by the NHC alone.[29]

Computational Study of Chain Termination. The above experimental investigation into the possible chain termination pathways involved in the polymerization of conjugate polar alkenes such as MMA and BMA by FLPs such as IMes/Al(C_6F_5)$_3$ (1/2) led to two types of possible chain ends: cyclic β-ketoester and δ-valerolactone (Scheme 3). The cyclic β-ketoester chain end could be generated by intramolecular backbiting cyclization involving nucleophilic attack of the activated antepenultimate ester group of the growing chain by the *C*-ester enolate active chain end (pathway a in Scheme 3), while the δ-valerolactone chain end could be generated by intramolecular backbiting cyclization involving nucleophilic attack of the activated adjacent ester group of the growing chain by the *O*-ester enolate active chain end (pathway b in Scheme 3). As differentiation of these two types of chains end became impossible by our current experimental methods using NMR and MS, we sought a solution to addressing this fundamental issue by computation studies.

DFT calculations were used to compare the two possible termination pathways with the chain growth pathway (Scheme 4). We started calculations on a model of the propagating species where the polymer chain is simulated with three MMA units terminated with a methyl group. In this model the LB is not included since it is assumed to be far enough away from the active center to have a noticeable influence on the mechanisms considered, and the overall model is more representative of a long PMMA chain. A comparison between the two possible

Scheme 4. Energetics (kcal/mol) of the β-Ketoester and δ-Valerolactone Chain Termination Pathways and of the Chain Growth (Numbers in Parentheses Are Free Energies)

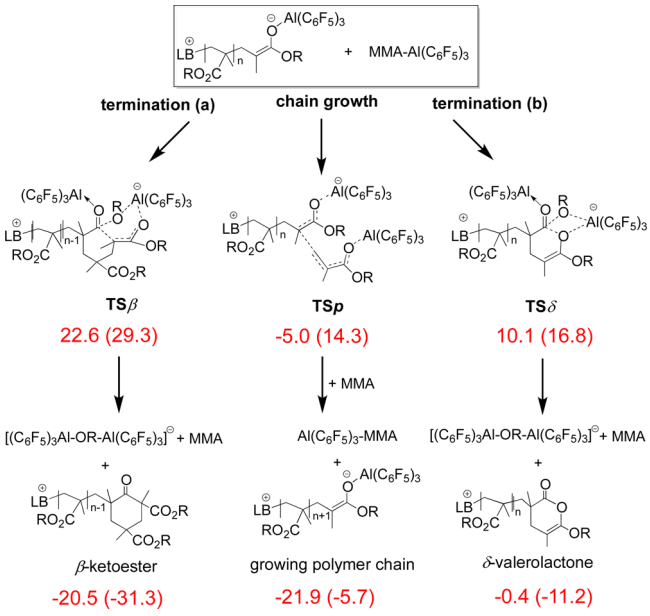

dx.doi.org/10.1021/ma5019389 | *Macromolecules* XXXX, XXX, XXX–XXX

chain termination pathways indicates that the δ-valerolactone termination pathway is clearly favored over the β-ketoester termination pathway, since transition state TSδ lies 12.5 kcal/mol below transition state TSβ, despite the fact that the β-ketoester termination product is thermodynamically favored by 20.1 kcal/mol. While the higher stability of the β-ketoester reflects the relative stability of the functional groups in the two termination products, the energy preference for TSδ over TSβ can be ascribed to the different nucleophilicity of the enolate C and O atoms, which attack the LA-activated C═O group of a previously added MMA molecule. Indeed, analysis of the natural atomic charges in the growing chain end (i.e., the starting structure at 0 kcal/mol) reveals a negative charge of −0.83*e* on the enolate oxygen atom that will be involved in the nucleophilic attack in TSδ and a negative charge of only −0.23*e* on the enolate carbon atom that will be involved in the nucleophilic attack in TSβ. This large difference in the atomic charge indicates a much higher nucleophilicity of the LA-bound oxygen relative to the carbon, which is consistent with the clearly lower energy barrier for the δ-valerolactone termination pathway. Incidentally, we also calculated the energy barrier for both the β-ketoester and δ-valerolactone termination pathways in a scenario where no LA is coordinated to the C═O group being attacked in backbiting; energy barriers at least 8.0 kcal/mol higher were found in both termination cases, showing the remarkable activating effect of the LA.

As for a comparison between the kinetically favored δ-valerolactone chain-termination pathway and the chain growth reaction, corresponding to the addition of a LA-activated MMA molecule to the growing polymer chain, the latter is largely favored in terms of potential energy, explaining why relatively high-MW polymers can be achieved by the current catalyst system. This conclusion was deduced from the results that the potential energy barrier for the chain growth, calculated as the energy difference between transition state TS*p* of Scheme 4 and the growing chain plus a LA-MMA adduct, is 15.1 kcal/mol lower than the potential energy barrier for the chain termination, calculated as the energy difference between transition state TSδ of Scheme 4 and a growing chain presenting a second LA coordinated to the C═O group of the penultimate MMA molecule. Indeed, this growing chain is the one present in the reaction media immediately after addition of a new LA-MMA adduct. Furthermore, due to the different molecularity of the addition (bimolecular) and of the considered chain termination reactions (unimolecular), this large difference in the potential energy barriers is reduced to only 2.5 kcal/mol when entropy effects, which disfavor the bimolecular chain growth transition state, are taken into account and the comparison is performed in terms of free energy barriers.[30]

A structural comparison of the TS geometry for the chain growth and the chain termination pathway along the δ-valerolactone pathway is depicted in Figure 9. In the chain growth transition state TS*p*, the bond distance of the emerging C−C bond, deriving from attack of the methylene C atom of the LA-MMA adduct by the enolate C atom of the growing chain, is 2.09 Å, while the Al−O bond involving the exiting LA group, 1.87 Å, is already slightly longer than the Al−O bond of the LA-MMA adduct that is going to be added to the growing chain, 1.82 Å. Overall, the two bulky LA moieties are well separated in space, minimizing steric repulsion. The δ-valerolactone termination transition state TSδ, instead, presents a highly concerted four-center geometry, with a very short

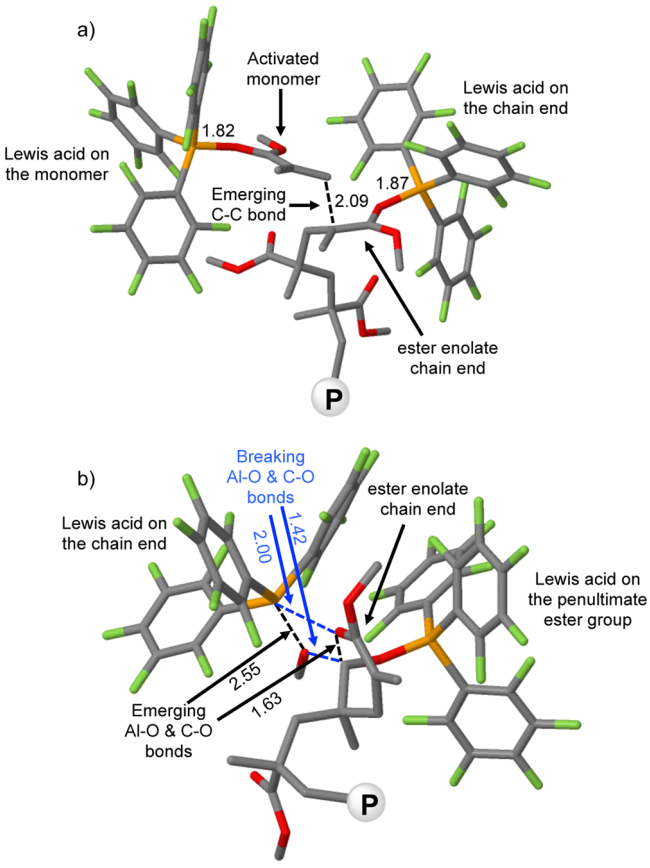

Figure 9. Geometries of the chain growth transition state TS*p* and the δ-valerolactone chain termination transition state TSδ. Relevant distances are reported in Å.

emerging C−O bond, 1.63 Å only, and the exiting LA molecule, originally bonded to the enolate atom of the chain end, already in the act of being transferred to the OMe group of the enolate chain end. The role of the second LA molecule, attached to the C═O of the penultimate MMA unit, is activating the C═O bond. Steric interaction between the two LA molecules is minimal, since they are oriented away from each other (cf. Figure 9).

CONCLUSIONS

In summary, this contribution investigated mechanistic aspects of conjugate-addition polymerization of conjugated polar alkenes by the [Al]-based FLPs by focusing on active propagating intermediate characterization, propagation kinetics, and chain termination pathways. In this context, we successfully isolated and structurally characterized the zwitterionic intermediate $IMes^{+}$-$CH_2C(Me)$═$(C_3H_2NO)Al(C_6F_5)_3^{-}$ (**2**), derived from FLP activation of *i*POx by IMes/$Al(C_6F_5)_3$, which simulates the active propagating species in such polymerization. Analogous intermediate I^tBu^{+}-$CH_2C(Me)$═$(C_3H_2NO)Al(C_6F_5)_3^{-}$ (**3**) was also generated from activation of *i*POx by $I^tBu/Al(C_6F_5)_3$, and I^tBu^{+}-CH_2CH═$(C_5H_4N)Al(C_6F_5)_3^{-}$ (**4**) was isolated from activation of 2-VP by $I^tBu/Al(C_6F_5)_3$. The structure of intermediate **2** is the first characterized active intermediate involved in the polymerization of *i*POx by FLPs and represents one of only a handful of structurally characterized zwitterionic intermediates that simulate the active propagating species for the Lewis pair polymerization of conjugate polar alkenes.

dx.doi.org/10.1021/ma5019389 | *Macromolecules* XXXX, XXX, XXX−XXX

Polymerization kinetics were performed on a prototype system most suitable for this study, the polymerization of 2-VP by the $I^tBu/Al(C_6F_5)_3$ FLP. The kinetic data revealed that the polymerization follows a zero-order dependence on monomer concentration and a first-order dependence on initiator (LB) and activator (LA) concentrations. Such kinetics imply a bimolecular, activated monomer propagation mechanism in that the C−C bond forming step via intermolecular Michael addition of the propagating species to the LA-activated monomer is the rate-limiting step, and the release of the LA catalyst from its coordinated last inserted monomer unit in the growing polymer chain to the incoming monomer is relatively fast.

The Lewis pair polymerization of conjugated polar alkenes by CLAs or FLPs is accompanied by competing chain-termination side reactions. The two possible chain-termination pathways were proposed: one that proceeds via intramolecular backbiting cyclization involving nucleophilic attack of the activated antepenultimate ester group of the growing chain by the *C*-ester enolate active chain end to generate a cyclic *β*-ketoester chain end and the other that proceeds via intramolecular backbiting cyclization involving nucleophilic attack of the activated adjacent ester group of the growing chain by the *O*-ester enolate active chain end to generate a *δ*-valerolactone chain end. Analyses of low molecular weight polymer samples produced by $IMes/Al(C_6F_5)_3$ with MALDI-TOF MS spectroscopy provided evidence for such chain termination side reactions but cannot conclusively state which process is operative in this polymerization. On the other hand, DFT calculations showed that the formation of cyclic *δ*-valerolactone-terminated chain ends is kinetically favored (lower energy barrier by 12.5 kcal/mol) but thermodynamically disfavored (less stable by 20.1 kcal/mol), as compared to the formation of *β*-ketoester-terminated chain ends.

■ ASSOCIATED CONTENT

Ⓢ Supporting Information

Single-crystal X-ray diffraction data, computational details, and additional figures. This material is available free of charge via the Internet at http://pubs.acs.org.

■ AUTHOR INFORMATION

Corresponding Authors

*E-mail: luigi.cavallo@kaust.edu.sa (L.C.).

*E-mail: eugene.chen@colostate.edu (E.Y.-X.C.).

Notes

The authors declare no competing financial interest.

■ ACKNOWLEDGMENTS

This work was supported by the National Science Foundation (NSF-1150792) for the study carried out at Colorado State University. L.C. thanks the HPC team of Enea for using the ENEA-GRID and the HPC facilities CRESCO in Portici, Italy. We thank Boulder Scientific Co. for the research gift of $B(C_6F_5)_3$ and Dr. Brian Newell for assistance on X-ray structural analysis.

■ REFERENCES

(1) Selected reviews: (a) Stephan, D. W.; Erker, G. *Chem. Sci.* **2014**, *5*, 2625−2641. (b) *Frustrated Lewis Pairs I & II*; Stephan, D. W., Erker, G., Eds.; Topics in Current Chemistry; Springer: New York, 2013, Vols. *332* and *334*. (c) Erker, G. *Pure Appl. Chem.* **2012**, *84*, 2203−2217. (d) Stephan, D. W. *Org. Biomol. Chem.* **2012**, *10*, 5740−5746. (e) Erker, G. *Dalton Trans.* **2011**, *40*, 7475−7483. (f) Stephan, D. W.; Erker, G. *Angew. Chem., Int. Ed.* **2010**, *49*, 46−76. (g) Stephan, D. W. *Dalton Trans.* **2009**, 3129−3136. (h) Stephan, D. W. *Org. Biomol. Chem.* **2008**, *6*, 1535−1539.

(2) Selected recent examples on activation of small molecules by FLPs: (a) Lawrence, E. J.; Oganesyan, V. S.; Hughes, D. L.; Ashley, A. E.; Wildgoose, G. G. *J. Am. Chem. Soc.* **2014**, *136*, 6031−6036. (b) Dobrovetsky, R.; Stephan, D. W. *J. Am. Chem. Soc.* **2013**, *135*, 4974−4977. (c) Sajid, M.; Elmer, L.-M.; Rosorius, C.; Daniliuc, C. G.; Grimme, S.; Kehr, G.; Erker, G. *Angew. Chem., Int. Ed.* **2013**, *52*, 2243−2246. (d) Appelt, C.; Slootweg, J. C.; Lammertsma, K.; Uhl, W. *Angew. Chem., Int. Ed.* **2013**, *52*, 4256−4259. (e) Bertini, F.; Lyaskovskyy, V.; Timmer, B. J. J.; de Kanter, F. J. J.; Lutz, M.; Ehlers, A. W.; Slootweg, J. C.; Lammertsma, K. *J. Am. Chem. Soc.* **2012**, *134*, 201−204. (f) Schäfer, A.; Reißmann, M.; Schäfer, A.; Saak, W.; Haase, D.; Müller, T. *Angew. Chem., Int. Ed.* **2011**, *50*, 12636−12638. (g) Lu, Z.; Cheng, Z.; Chen, Z.; Weng, L.; Li, Z. H.; Wang, H. *Angew. Chem., Int. Ed.* **2011**, *50*, 12227−122231. (h) Ekkert, O.; Kehr, G.; Fröhlich, R.; Erker, G. *J. Am. Chem. Soc.* **2011**, *133*, 4610−4616. (i) Marwitz, A. J. V.; Dutton, J. L.; Mercier, L. G.; Piers, W. E. *J. Am. Chem. Soc.* **2011**, *133*, 10026−10029. (j) Appelt, C.; Westenberg, H.; Bertini, F.; Ehlers, A. W.; Slootweg, J. C.; Lammertsma, K.; Uhl, W. *Angew. Chem., Int. Ed.* **2011**, *50*, 3925−3928. (k) Grimme, S.; Kruse, H.; Goerigk, L.; Erker, G. *Angew. Chem., Int. Ed.* **2010**, *49*, 1402−1405. (l) Inés, B.; Holle, S.; Goddard, R.; Alcarazo, M. *Angew. Chem., Int. Ed.* **2010**, *49*, 8389−8391. (m) Mömming, C. M.; Otten, E.; Kehr, G.; Fröhlich, R.; Grimme, S.; Stephan, D. W.; Erker, G. *Angew. Chem., Int. Ed.* **2009**, *48*, 6643−6646. (n) Chase, P. A.; Stephan, D. W. *Angew. Chem., Int. Ed.* **2008**, *47*, 7433−7437. (o) Holschumacher, D.; Bannenberg, T.; Hrib, C. G.; Jones, P. G.; Tamm, M. *Angew. Chem., Int. Ed.* **2008**, *47*, 7428−7432. (p) Sumerin, V.; Schulz, F.; Nieger, M.; Leskela, M.; Repo, T.; Rieger, B. *Angew. Chem., Int. Ed.* **2008**, *47*, 6001−6003.

(3) Selected recent examples on catalytic hydrogenation by FLPs: (a) Chernichenko, K.; Madarász, A.; Pápai, I.; Nieger, M.; Leskelä, M.; Repo, T. *Nat. Chem.* **2013**, *5*, 718−723. (b) Greb, L.; Daniliuc, C.-G.; Bergander, K.; Paradies, J. *Angew. Chem., Int. Ed.* **2013**, *52*, 5876−5879. (c) Hounjet, L. J.; Bannwarth, C.; Garon, C. N.; Caputo, C. B.; Grimme, S.; Stephan, D. W. *Angew. Chem., Int. Ed.* **2013**, *52*, 7492−7495. (d) Chen, D.; Wang, Y.; Klankermayer, J. *Angew. Chem., Int. Ed.* **2010**, *49*, 9475−9478. (e) Erős, G.; Mehdi, H.; Pápai, I.; Rokob, T. A.; Király, P.; Tárkányi, G.; Soós, T. *Angew. Chem., Int. Ed.* **2010**, *49*, 6559−6563. (f) Miller, A. J. M.; Labinger, J. A.; Bercaw, J. E. *J. Am. Chem. Soc.* **2010**, *132*, 3301−3303. (g) Ashley, A. W.; Thompson, A. L.; O'Hare, D. *Angew. Chem., Int. Ed.* **2009**, *48*, 9839−9843. (h) Axenov, K. V.; Kehr, G.; Fröhlich, R.; Erker, G. *J. Am. Chem. Soc.* **2009**, *131*, 3454−3455.

(4) Selected recent examples on new reactivity/reaction development with FLPs: (a) Wang, X.; Kehr, G.; Daniliuc, C. G.; Erker, G. *J. Am. Chem. Soc.* **2014**, *136*, 3293−3303. (b) Rocchigiani, L.; Giancaleoni, G.; Zuccaccia, C.; Macchioni, A. *J. Am. Chem. Soc.* **2014**, *136*, 112−115. (c) Ménard, G.; Hatnean, J. A.; Cowley, H. J.; Lough, A. J.; Rawson, J. M.; Stephan, D. W. *J. Am. Chem. Soc.* **2013**, *135*, 6446−6449. (d) Sajid, M.; Kehr, G.; Wiegand, T.; Eckert, H.; Schwickert, C.; Pöttgen, R.; Cardenas, A. J. P.; Warren, T. H.; Fröhlich, R.; Daniliuc, C. G.; Erker, G. *J. Am. Chem. Soc.* **2013**, *135*, 8882−8895. (e) Cardenas, A. J. P.; Culotta, B. J.; Warren, T. H.; Grimme, S.; Stute, A.; Fröhlich, R.; Kehr, G.; Erker, G. *Angew. Chem., Int. Ed.* **2011**, *50*, 7567−7571. (f) Chapman, A. M.; Haddow, M. F.; Wass, D. F. *J. Am. Chem. Soc.* **2011**, *133*, 8826−8829. (g) Ménard, G.; Stephan, D. W. *Angew. Chem., Int. Ed.* **2011**, *50*, 8396−8399. (h) Zhao, X.; Stephan, D. W. *J. Am. Chem. Soc.* **2011**, *133*, 12448−12450. (i) Ménard, G.; Stephan, D. W. *J. Am. Chem. Soc.* **2010**, *132*, 1796−1797. (j) Alcarazo, M.; Gomez, C.; Holle, S.; Goddard, R. *Angew. Chem., Int. Ed.* **2010**, *49*, 5788−5791. (k) Berkefeld, A.; Piers, W. E.; Parvez, M. *J. Am. Chem. Soc.* **2010**, *132*, 10660−10661. (l) Mömming, C. M.; Kehr, G.; Wibbeling, B.; Fröhlich, R.; Schirmer, B.; Grimme, S.; Erker, G. *Angew. Chem., Int. Ed.* **2010**, *49*, 2414−2417.

(5) Chen, E. Y.-X. *Top. Curr. Chem.* **2013**, *334*, 239−260.

(6) (a) Zhang, Y.; Miyake, G. M.; John, M. G.; Falivene, L.; Caporaso, L.; Cavallo, L.; Chen, E. Y.-X. *Dalton Trans.* **2012**, *41*, 9119−9134. (b) Zhang, Y.; Miyake, G. M.; Chen, E. Y.-X. *Angew. Chem., Int. Ed.* **2010**, *49*, 10158−10162.
(7) Gowda, R. R.; Chen, E. Y.-X. *Encycl. Polym. Sci. Technol.* **2013**, DOI: 10.1002/0471440264.pst606.
(8) Xu, T.; Chen, E. Y.-X. *J. Am. Chem. Soc.* **2014**, *136*, 1774−1777.
(9) He, J.; Zhang, Y.; Chen, E. Y.-X. *Synlett* **2014**, *25*, 1534−1538.
(10) Piedra-Arroni, E.; Ladavière, C.; Amgoune, A.; Bourissou, D. *J. Am. Chem. Soc.* **2013**, *135*, 13306−13309.
(11) Sajid, M.; Stute, A.; Cardenas, A. J. P.; Culotta, B. J.; Hepperle, J. A. M.; Warren, T. H.; Schirmer, B.; Grimme, S.; Studer, A.; Daniliuc, C. G.; Fröhlich, R.; Petersen, J. L.; Kehr, G.; Erker, G. *J. Am. Chem. Soc.* **2012**, *134*, 10156−10168.
(12) Jia, Y.-B.; Ren, W.-M.; Liu, S.-J.; Xu, T.; Wang, Y.-B.; Lu, X.-B. *ACS Macro Lett.* **2014**, *3*, 896−899.
(13) Jia, Y.-B.; Wang, Y.-B.; Ren, W.-M.; Xu, T.; Wang, J.; Lu, X.-B. *Macromolecules* **2014**, *47*, 1966−1972.
(14) Allen, R. D.; Long, T. E.; McGrath, J. E. *Polym. Bull.* **1986**, *15*, 127−134.
(15) Feng, S.; Roof, G. R.; Chen, E. Y.-X. *Organometallics* **2002**, *21*, 832−839.
(16) (a) Lee, C. H.; Lee, S. J.; Park, J. W.; Kim, K. H.; Lee, B. Y.; Oh, J. S. *J. Mol. Catal., A: Chem.* **1998**, *132*, 231−239. (b) Biagini, P.; Lugli, G.; Abis, L.; Andreussi, P. U.S. Pat. US5,602269, 1997.
(17) SHELXTL, Version 6.12; Bruker Analytical X-ray Solutions, Madison, WI, 2001.
(18) (a) Chen, X.; Caporaso, L.; Cavallo, L.; Chen, E. Y.-X. *J. Am. Chem. Soc.* **2012**, *134*, 7278−7281. (b) Caporaso, L.; Cavallo, L. *Macromolecules* **2008**, *41*, 3439−3445. (c) Caporaso, L.; Gracia-Budrìa, J.; Cavallo, L. *J. Am. Chem. Soc.* **2006**, *128*, 16649−16654.
(19) Becke, A. D. *Phys. Rev. A* **1988**, *38*, 3098−3100.
(20) (a) Perdew, J. P. *Phys. Rev. B* **1986**, *33*, 8822−8824. (b) Perdew, J. P. *Phys. Rev. B* **1986**, *34*, 7406−7406.
(21) Weigend, F.; Ahlrichs, R. *Phys. Chem. Chem. Phys.* **2005**, *7*, 3297−3305.
(22) (a) Tomasi, J.; Mennucci, B.; Cammi, R. *Chem. Rev.* **2005**, *105*, 2999−3093. (b) Barone, B.; Cossi, M. *J. Phys. Chem. A* **1998**, *102*, 1995−2001.
(23) Zhang, N.; Salzinger, S.; Soller, B. S.; Rieger, B. *J. Am. Chem. Soc.* **2013**, *135*, 8810−8813.
(24) Chen, E. Y.-X. *Chem. Rev.* **2009**, *109*, 5157−5214.
(25) (a) Stojcevic, G.; Kim, H.; Taylor, N. J.; Marder, T. B.; Collins, S. *Angew. Chem., Int. Ed.* **2004**, *43*, 5523−5526. (b) Li, Y.; Ward, D. G.; Reddy, S. S.; Collins, S. *Macromolecules* **1997**, *30*, 1875−1883.
(26) (a) Zhang, Y.; Chen, E. Y.-X. *Macromolecules* **2008**, *41*, 6353−6360. (b) Zhang, Y.; Chen, E. Y.-X. *Macromolecules* **2008**, *41*, 36−42.
(27) Mariott, W. R.; Rodriguez-Delgado, A.; Chen, E. Y.-X. *Macromolecules* **2006**, *39*, 1318−1327.
(28) Baskaran, D. *Prog. Polym. Sci.* **2003**, *28*, 521−581.
(29) Zhang, Y.; Schmitt, M.; Falivene, L.; Caporaso, L.; Cavallo, L.; Chen, E. Y.-X. *J. Am. Chem. Soc.* **2013**, *135*, 17925−17942.
(30) Haras, A.; Anderson, G. D. W.; Michalak, A.; Rieger, B.; Ziegler, T. *Organometallics* **2006**, *25*, 4491−4497.